Supplemental Data

Yoon et al. Structure and Mechanism of receptor sharing by the IL-10R2 common chain

Fig S1

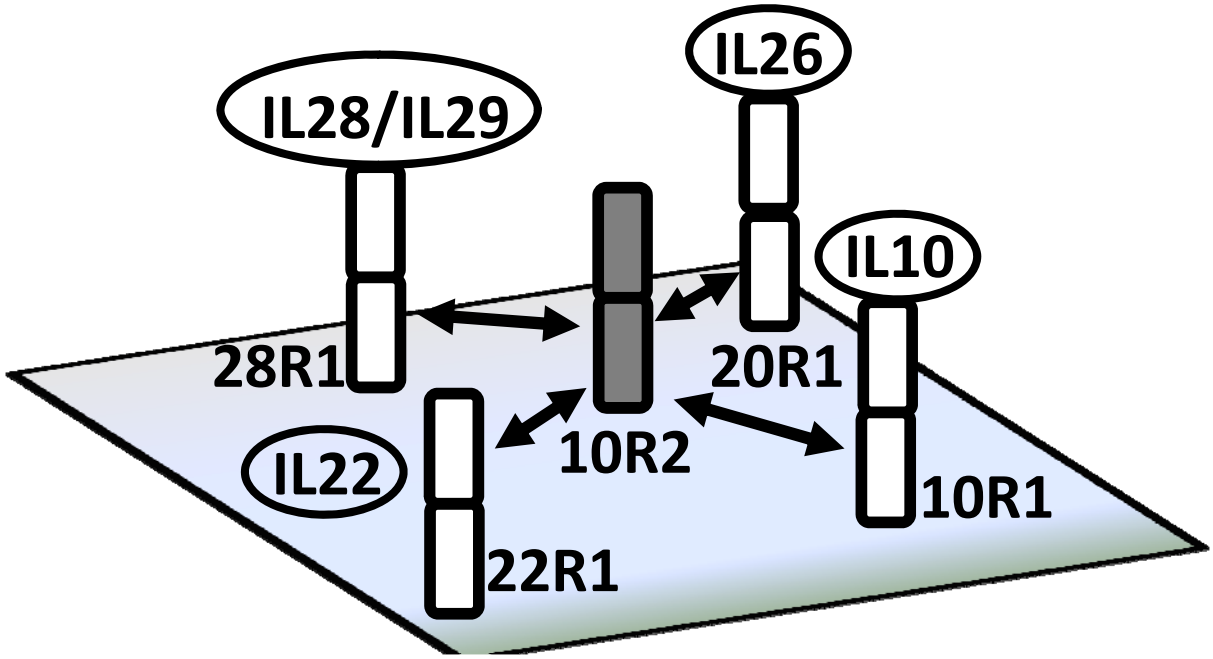

Fig S2

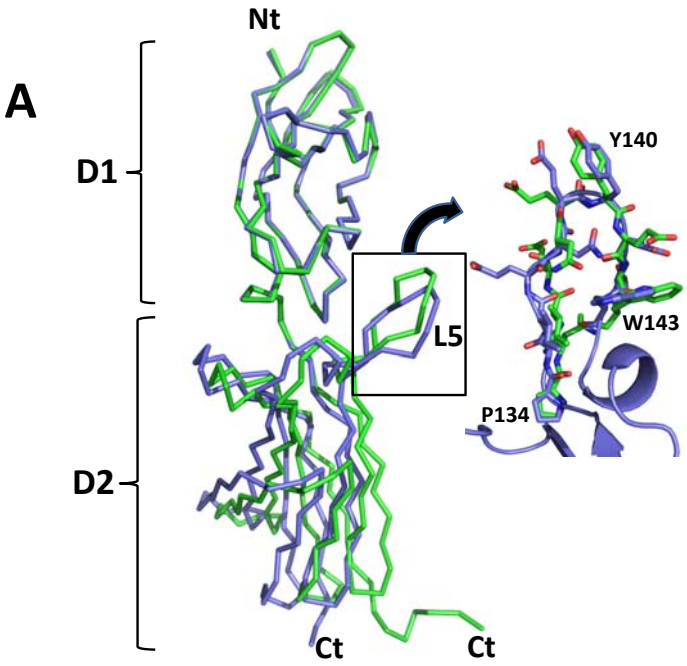

D1-D2 Inter-domain Angles

Receptor	Elbow	Twist	Swivel
10R2 (chain A)	95.1	118.3	126.8
10R2 (chain B)	96.0	122.9	132.8
10R1	90.7	130.2	133.0
22R1 (Chain A)	91.7	133.6	101.3

All angles in degrees. Definitions of each angle are described in Deivanayagam et al. (Deivanayagam et al.. 1999)

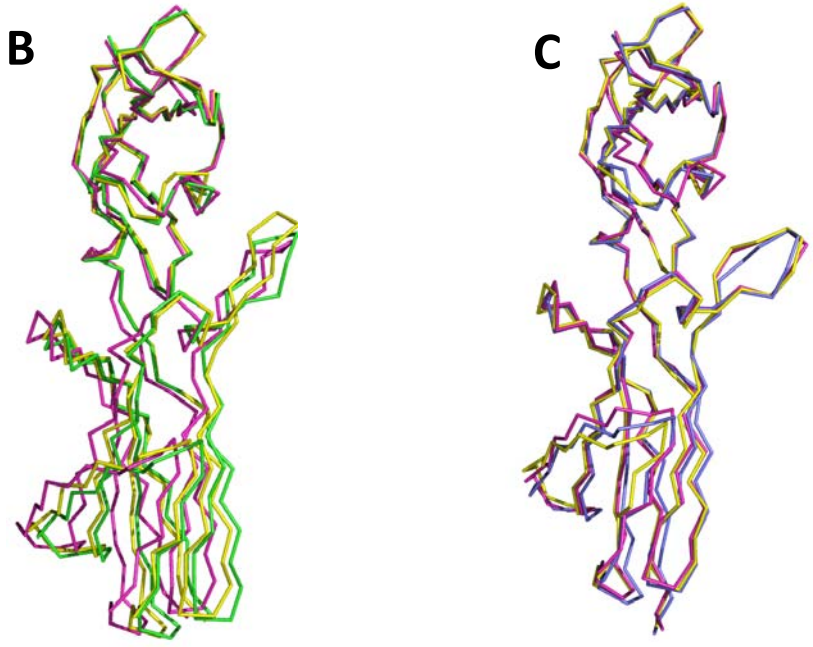

Fig S3

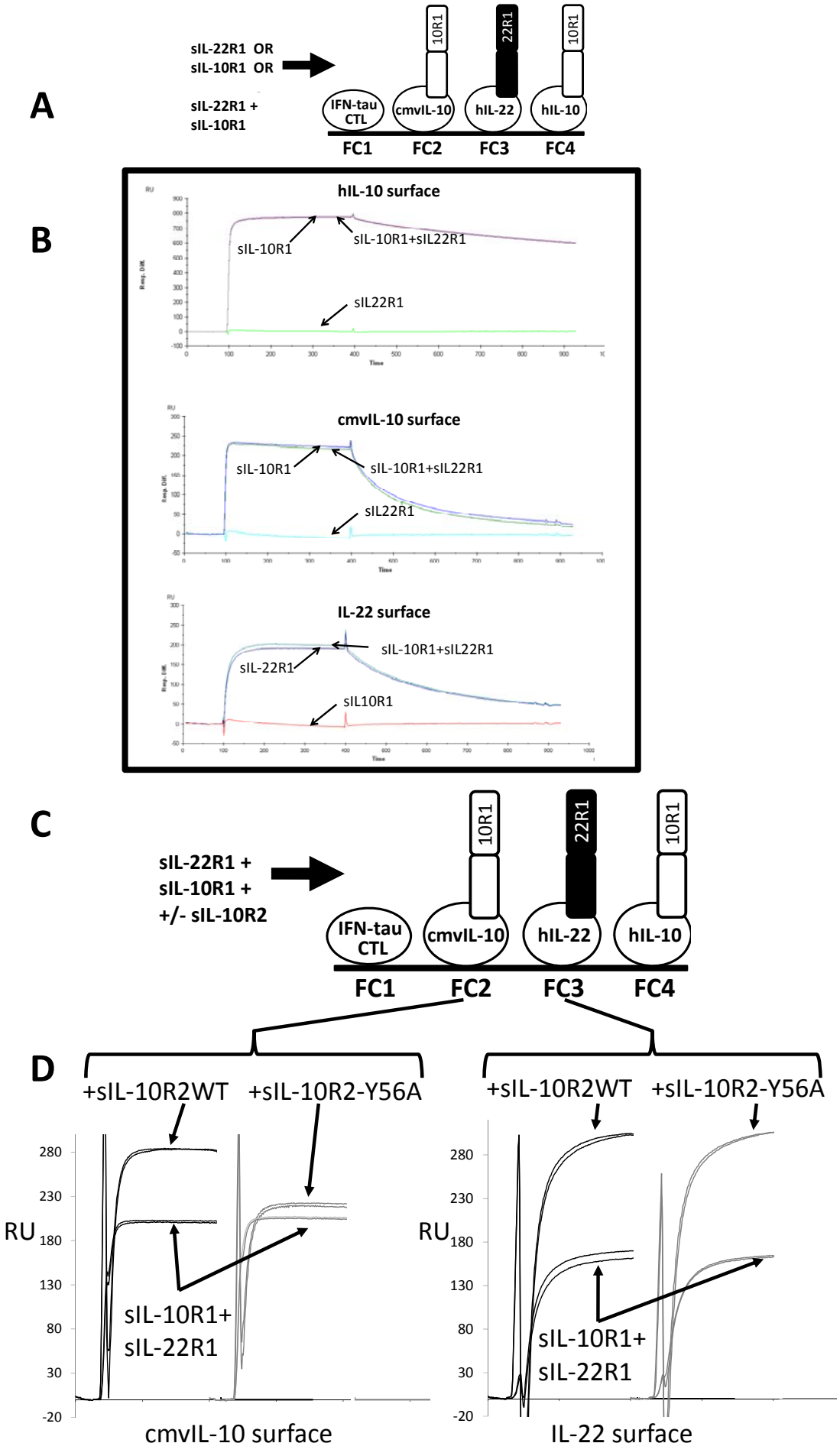
A
sIL-22R1 OR
sIL-10R1 OR
sIL-22R1 +
sIL-10R1
10R1
22R1
10R1
IFN-tau CTL
cmvIL-10
hIL-22
hIL-10
FC1
FC2
FC3
FC4
B
hIL-10 surface
sIL-10R1
sIL-10R1+sIL22R1
sIL22R1
cmvIL-10 surface
sIL-10R1
sIL-10R1+sIL22R1
sIL22R1
IL-22 surface
sIL-22R1
sIL-10R1+sIL22R1
sIL10R1
C
sIL-22R1 +
sIL-10R1 +
+/- sIL-10R2
10R1
22R1
10R1
IFN-tau CTL
cmvIL-10
hIL-22
hIL-10
FC1
FC2
FC3
FC4
D
+sIL-10R2WT
+sIL-10R2-Y56A
RU
280
230
180
130
80
30
-20
sIL-10R1+
sIL-22R1
cmvIL-10 surface
+sIL-10R2WT
+sIL-10R2-Y56A
RU
280
230
180
130
80
30
-20
sIL-10R1+
sIL-22R1
IL-22 surface

Fig S4

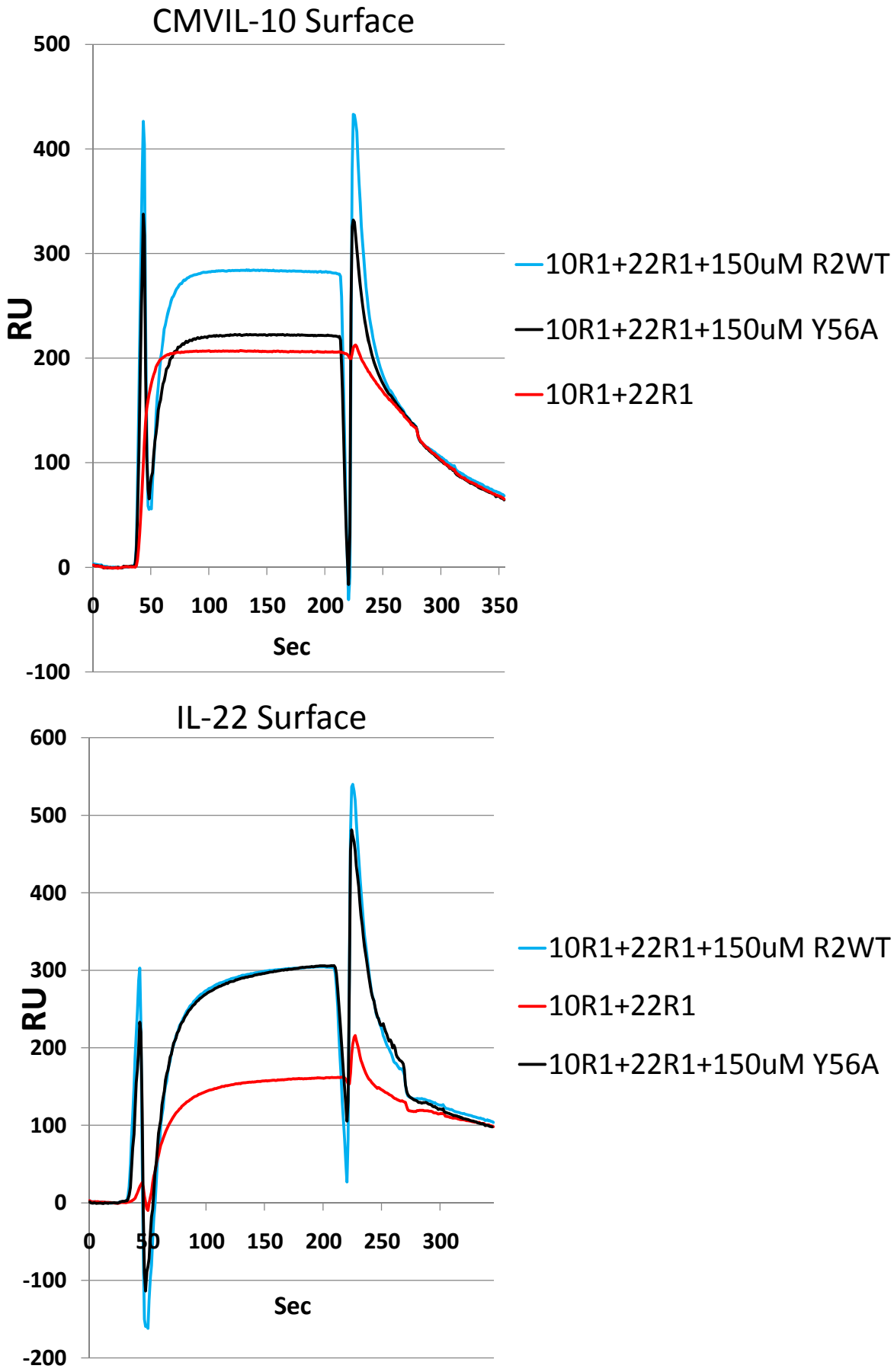
CMVIL-10 Surface
500
400
300
200
100
0
-100
RU
0
50
100
150
200
250
300
350
Sec
10R1+22R1+150uM R2WT
10R1+22R1+150uM Y56A
10R1+22R1
IL-22 Surface
600
500
400
300
200
100
0
-100
-200
RU
0
50
100
150
200
250
300
Sec
10R1+22R1+150uM R2WT
10R1+22R1
10R1+22R1+150uM Y56A

FIG S5

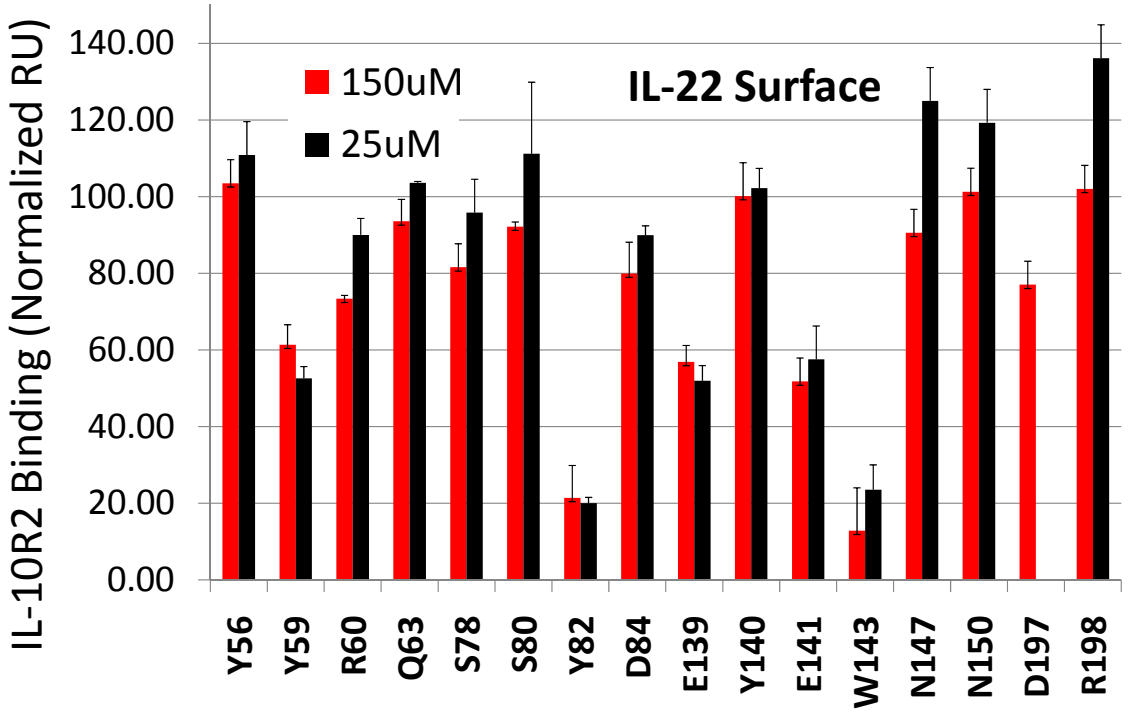
IL-22 Surface
150uM
25uM
IL-10R2 Binding (Normalized RU)
140.00
120.00
100.00
80.00
60.00
40.00
20.00
0.00
Y56
Y59
R60
Q63
S78
S80
Y82
D84
E139
Y140
E141
W143
N147
N150
D197
R198

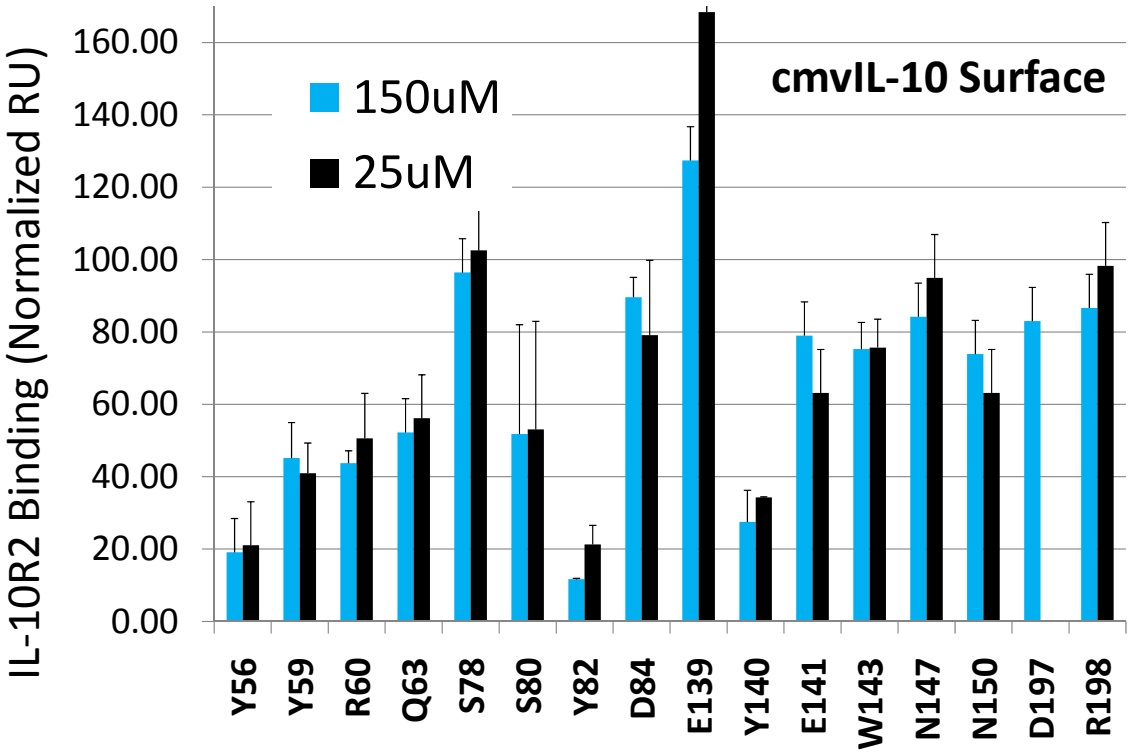
cmvIL-10 Surface
150uM
25uM
IL-10R2 Binding (Normalized RU)
160.00
140.00
120.00
100.00
80.00
60.00
40.00
20.00
0.00
Y56
Y59
R60
Q63
S78
S80
Y82
D84
E139
Y140
E141
W143
N147
N150
D197
R198

FIG S6

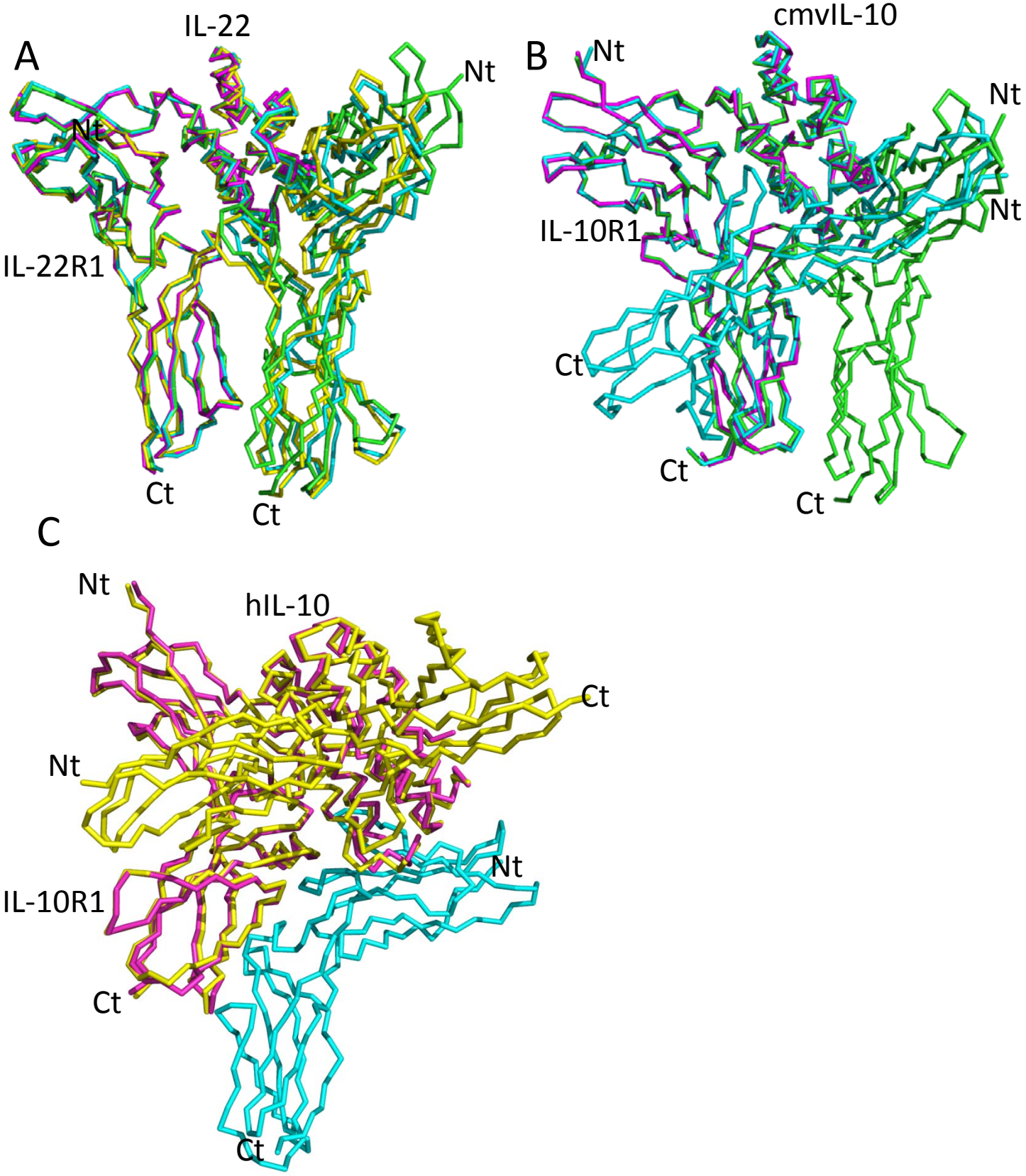
A
IL-22
Nt
Nt
IL-22R1
Ct
Ct
B
cmvIL-10
Nt
Nt
Nt
IL-10R1
Ct
Ct
Ct
C
Nt
hIL-10
Ct
Nt
Nt
IL-10R1
Ct
Ct

Fig S7

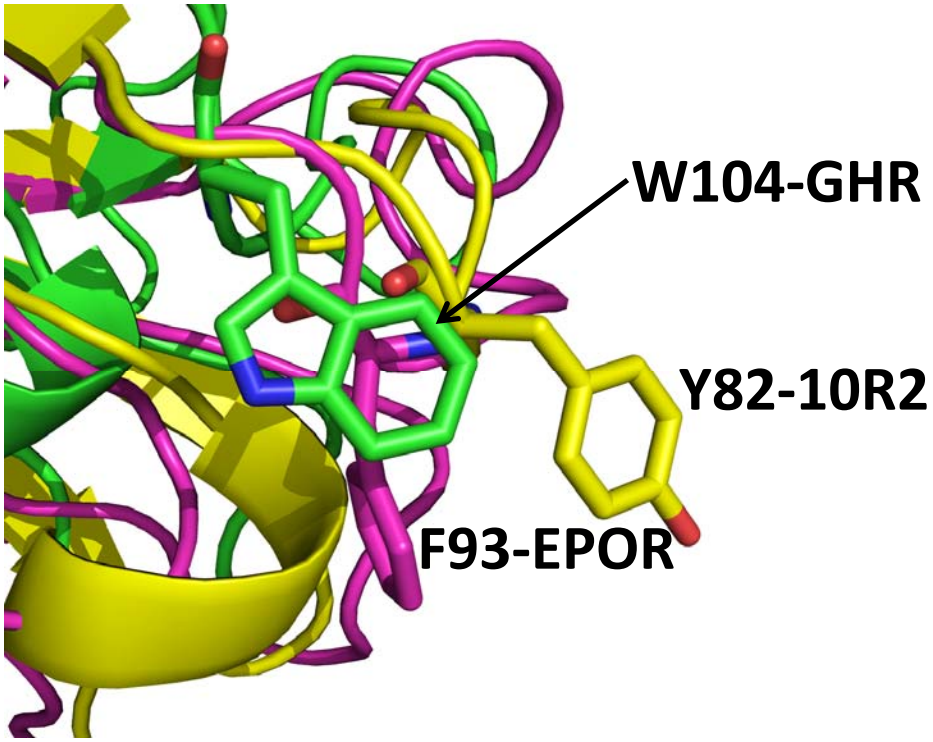

Supplement Figure Legends

Figure S1. Schematic diagram of sIL-10R2 receptor sharing. Cytokines are denoted by ovals.

Figure S2. Domain orientations of non-crystallographically related sIL-10R2 chains. (A) The D1 domains of sIL-10R2 chain A (green) and chain B (purple) are shown with D1 domains superimposed (r.m.s.d. = 0.35Å). The inset in the Figure shows the L5 loop (residues 134-143), which exhibits different conformations in chains A and B due to crystal contacts. To generate the inset figure for the L5 loop, the D2 domains of the A and B chains were superimposed (r.m.s.d = 0.68Å). The table below Figure S2A provides a comparison of elbow, twist, and swivel angles as defined by Deivanayagam et al. (Deivanayagam et al., 2000). **(B)** D1 superposition of sIL-10R2 from IL-22 (C-A-R18-S1, yellow) and cmvIL-10 (C-A-R13-S1, magenta) ternary complexes (Table S2) onto Chain A of sIL-10R2 (green). **(C)** D1 superposition of sIL-10R2 from IL-22 (C-B-R15-S6, yellow) and cmvIL-10 (C-B-R12-S1, magenta) ternary complexes (Table S2) onto Chain B of sIL-10R2 (purple).

Figure S3. R1 chain specificity and IL-10R2 binding analyses. (A) Experimental design used to test the binding specificity of sIL-22R1 and sIL-10R1 chains for cmvIL-10, IL-22, and hIL-10 surfaces. **(B)** Sensorgrams for each surface are shown with injections of sIL-22R1, sIL-10R1, and sIL-22R1+sIL-10R1. **(C)** Schematic diagram of the IL-10R2 binding experiment. (**D**) Sensorgrams are shown for injections of sIL-10R1+sIL-22R1 +/- sIL-10R2WT or +/- sIL-10R2-Y56A over cmvIL-10 (left) and IL-22 (right) chip surfaces.

Figure S4. Complete sensorgrams with the dissociation phase. Sensorgrams, showing the large bulk shifts due to high sIL-10R2 protein concentration, and the off-rates of the receptors, are shown for the experiment in Figure S3D.

Figure S5. Relative sIL-10R2 binding to IL-22 and cmvIL-10 BCs at 25μM and 150μM concentrations. To further validate the initial findings of the SPR study, a 25μM sIL-10R2 concentration (WT and mutants) was evaluated by SPR and analyzed as described for the 150μM concentration. No significant differences were observed between the data collected at 25μM and 150μM on the cmvIL-10 and IL-22 surfaces. The errors in the data collected on the hIL-10 surface were >55% and were not used for further analysis.

Figure S6. Haddock sIL-10R2 docking solutions. Alpha carbon representations of IL-22, cmvIL-10, and hIL-10 docking solutions listed in Table S2 and labeled by Chain (C), run number (R), and solution number (S) (See Table 2). IL-22/sIL-22R1, cmvIL-10/sIL-10R1, and hIL-10/sIL-10R1 crystal structures are colored magenta. **(A)** IL-22 TC docking solutions C-A-R18-S1, B-R15-S1, and C-B-R15-S6 are colored yellow, cyan, and green, respectively. **(B)** cmvIL-10 TC docking solutions C-A-R13-S1 and C-B-R12-S1 are colored cyan and green, respectively. **(C)** Best Haddock score solutions from the hIL-10 docking experiments. C-A-R22-S1 and C-B-R21-S1 are colored cyan and yellow, respectively.

Figure S7. Comparison of sIL-10R2-D1-Y82 with EPOR and growth hormone receptor (GHR). Close up view of IL-10R2 D1 (yellow), EPOR (magenta), and GHR (green) showing structural divergence of $F93^{EPOR}$ and $W104^{GHR}$ from sIL-10R2 Y82.

Table S1. Haddock AIR restraints.

IL-22BC*		sIL-10R2		cmvIL-10BC**		sIL-10R2		hIL-10BC***		sIL-10R2	
A	P	A	P	A	P	A	P	A	P	A	P
Y51	M58	Y59	R60	Q24	D25	Y56	E141	R24	N21	Y56	D84
N54	K61	Y82	S80	R32	V28	Y59	N150	R32	D25	Y59	E141
R55	E62	E139	D84		T29	R60	D197		D28	R60	N150
Y114		E141	D109		S93	Q63	R198		T31	Y82	D197
E117		W143	Y140			S80			S93	Y140	R198
		Y173	N150			Y82				W143	
			D197			Y140					
			R198								

A = Active residues, P = Passive residues, BC=binary complex. IL-22BC, cmvIL-10BC, hIL-10BC correspond to pdbids 3DGC, 1LQS, and 1Y6K, respectively.

Table S2. Haddock Docking Solutions.

Binary Complex	R2 Chain	run#	# of clusters*	cluster #	#strucs in cluster	Solut. #**	Haddock score	r.m.s.d. BC***	r.m.s.d. R2	C-term dist (Å)****	buried surface (A^2)
IL-22/IL-22R1	A	18	4	1	180	1	-166.6	0.74	0.84	29.1	1,214
IL-22/IL-22R1	B	15	6	2	34	1	-152.3	0.78	0.85	30.4	1,132
IL-22/IL-22R1	**B**	**15**	**6**	**4**	**19**	**6**	**-123.4**	**0.67**	**0.85**	**35.2**	**1,225**
cmv10/IL-10R1	A	13	11	1	84	1	-110.9	0.68	0.92	48.7	1,092
cmv10/IL-10R1	**B**	**12**	**10**	**1**	**55**	**1**	**-178.2**	**0.64**	**0.85**	**22.6**	**1,539**
hIL-10/IL-10R1	A	22	16	--	1	1	-138.7	1.05	0.85	33.4	1,130
hIL-10/IL-10R1	B	21	14	--	1	1	-124.8	0.98	0.8	94.2	1,219

* Total # of clusters for a given run using a 7.5Å cut off and requiring at least 4 structures to form a cluster.

** Overall ranking of the solution based on Haddock Score

*** BC = binary complex. r.m.s.d. for Ca atoms, relative to crystal structures

**** distance between C-terminal residues IL-10R1 Cα T206/IL-10R2 CαT194 or IL-22R1 Cα L222 /IL-10R2 Cα T194

Bolded solutions described in more detail in the text. Graphical comparison of solutions shown in Fig S6.

Surface area buried by sIL-10R2 into the IL-22/sIL-22R1 and cmvIL-10/sIL-10R1 complexes.

Table S3. Hydrogen bonds* in the IL-22 and cmvIL-10 ternary complexes (TCs).

Chain B-R15-S6								Chain B-R12-S1							
sIL-10R2				IL-22/IL-22R1			D	sIL-10R2				cmvIL-10/IL-10R1			D
								56	TYR	OH	....	89	THR	O	2.9
								59	TYR	OH	....	99	GLU	OE1	2.9
63	GLN	NE2	....	109	ASP	OD2	2.9								
78	SER	OG	....	116	GLN	OE1	2.9								
80	SER	OG	....	116	GLN	O	2.6	80	SER	OG	....	93	SER	O	2.8
								80	SER	OG	....	97	THR	OG1	3.2
81	LYS	N	....	117	GLU	OE1	2.8	81	LYS	N	....	25	ASP	OD2	2.6
								81	LYS	NZ	....	25	ASP	OD1	2.6
								85	HIS	NE2	....	96	SER	OG	3
128	HIS	ND1	....	173r	ARG	O	3	128	HIS	ND1	....	174r	SER	OG	2.8
137	GLU	O	....	51	TYR	OH	2.8								
139	GLU	OE1	....	55	ARG	NH1	2.7	139	GLU	OE1	....	32	ARG	NE	2.7
139	GLU	OE1	....	55	ARG	NH2	3.2								
139	GLU	OE2	....	114	TYR	OH	2.7								
141	GLU	OE1	....	54	ASN	ND2	3	141	GLU	OE1	....	187r	SER	OG	2.6
								141	GLU	OE1	....	163r	LYS	NZ	2.7
								141	GLU	OE2	....	185r	LYS	NZ	2.6
								142	THR	O	....	163r	LYS	NZ	3.1
								147	ASN	OD1	....	163r	LYS	NZ	2.9
								147	ASN	ND2	....	145r	GLU	OE1	2.7
								150	ASN	ND2	....	18	ASP	OD2	3
173	TYR	OH	....	168r	GLU	OE1	2.7								
173	TYR	OH	....	178r	HIS	ND1	2.7	174	ASP	OD2	....	162r	LYS	NZ	2.7

***** hydrogen bonds calculated with hbplus (McDonald and Thornton, 1994)**.** D = distance in Å, "r" distinguishes receptor residues from ligand residues in the BCs.

Table S4. Summary of final* IL-22 and cmvIL-10 TCs.

	IL-22TC		cmvIL-10TC	
	buried surface	# of H-bonds**	buried surface	# of H-bonds*
sIL-10R2 L2	280	1	346	2
sIL-10R2 L3	280	3	280	5
sIL-10R2 L5	350	5	546	8
sIL-10R2 : cytokine	910	9	835	8
sIL-10R2:R1 chain	315	3	705	7
Site 1***	808	12	990	16
Site 2	910	9	1172	15
Site 3	315	3	368	2
Site 2 + Site 3	1225	12	1540	17

* bolded complexes in Table S2

** hydrogen bonds calculated with hbplus (McDonald and Thornton, 1994)

*** From reference Jones et al., 2008

Supplemental Experimental Procedures

SPR studies.

SPR studies were performed as previously described by Yoon et al. (Yoon et al., 2006) except sIL-10R1 and sIL-22R1 were mixed together prior to injection over CM-5 chip surfaces coupled with IL-22, cmvIL-10, and hIL-10 (Fig S3). To ensure sIL-10R1 and sIL-22R1 were specific, solutions of 500nM sIL-22R1, 1μM sIL-10R1 and 500nM sIL-22R1+ 1μM sIL-10R1 were injected over the CM-5 chips coupled with IL-22, cmvIL-10, and hIL-10 as shown in Figure S3B. These experiments validated that equivalent RU values (e.g. sIL-10R1 vs. sIL-10R1+sIL-22R1 on the cmvIL-10 and hIL-10 surfaces) could be obtained using mixtures of sIL-10R1 and sIL-22R1. This allowed us to characterize sIL-10R2 alanine mutants to multiple binary complexes at the same time, as shown in Figure S3C and S3D. The complete sensorgrams for sIL-10R2 and Y56A, showing the dissociation of the receptors from the surface, is shown in Figure S4. To ensure the high concentrations of sIL-10R2 used in the experiments did not cause artifacts, the data shown in Figure 3 was re-collected at sIL-10R2 concentrations of 25μM. Error estimates for this dataset were 9%, 13% and >55% for IL-22, cmvIL-10, and hIL-10 chip surfaces, respectively. As seen in Figure S5, there is no significant difference in the IL-22 and cmvIL-10 data collected at 150μM and 25μM.

Haddock Docking Studies.

The two sIL-10R2 chains in the asymmetric unit of the crystals exhibit D1-D2 inter-domain angles that differ as described in Figure S2. Thus, docking studies were performed using chain A and chain B (Table S2). Ambiguous interaction restraints (AIRs, Table S1) were generated from the mutagenesis data. In addition, mainchain conformational variation of the cytokine/R1 binary complexes (IL-22/sIL-22R1 (pdbid 3DGC, chains L/R), cmvIL-10/sIL-10R1 (pdbid 1LQS, chains L/R) and hIL-10/sIL-10R1 (1Y6K)) was minimized by using unambiguous distance restraints. Unambiguous restraints for hIL-10/sIL-10R1 consisted of Cα distances between $D142^{hIL\text{-}10}$ and every other Cα atom in the hIL-10/sIL-10R1 complex. Similarly, $E142^{cmvIL\text{-}10}$ and $E166^{IL\text{-}22}$ were used to generate equivalent distance restraint tables for cmvIL-10/sIL-10R1 and IL-22/sIL-22R1 complexes, respectively. Only ½ of the cmvIL-10/sIL-10R1 and hIL-10/sIL-10R1 dimeric complexes (e.g. 1 domain of IL-10 and 1 sIL-10R1 chain) were used for all docking studies except one experiment using the full hIL-10 dimer and one sIL-10R1 as noted in the text.

IL-10R2 docking solutions output by HADDOCK were clustered to identify structurally equivalent solutions. As shown in Table S2, solutions formed 4 to 16 clusters depending on the binary complex used in the experiment. Individual clusters were analyzed for three main criteria. First, correct solutions were required to have the sIL-10R2 C-terminus oriented towards the putative position of the cell membrane and < 40Å from the C-terminus of the sIL-22R1 or sIL-10R1 chain. Second, correct solutions were expected to have low HADDOCK scores (e.g. top ranking solutions) in a given experiment. Finally, structures passing these requirements were further characterized by computer graphics to determine the docking solution most consistent with the mutagenesis data in Figure 3 and previously described in the literature (Logsdon et al., 2004; Wolk et al., 2004; Wu et al., 2008; Yoon et al., 2006). For example, if a residue important for sIL-10R2 binding did not participate in any contacts with cytokine or R1 chain, this solution was considered inferior to other possible solutions.

The top ranked docking solutions for each binary complex is shown in Figure S6. Essentially equivalent docking solutions, with low Haddock scores, were obtained when sIL-10R2 chain A, or chain B, was docked onto IL-22/sIL-22R1 (Table S2, Fig S6). An additional distinct solution formed a separate cluster (cluster 4) that contained the sixth overall best HADDOCK score (Table S2). These three structures (Chain (C-) A, Run (-

R) 18, solution (-S) 1, C-B-R15-S1, and C-B-R15-S 6) were evaluated in more detail. Graphical analyses of these complexes argued that C-B-R15-S6 provided the best overall fit to the mutagenesis data. In particular, $Y59^{sIL\text{-}10R2}$ and $R60^{sIL\text{-}10R2}$ form more extensive contacts with IL-22 than in the other complexes. $E141^{sIL\text{-}10R2}$ forms direct hydrogen bonds with $N54^{IL\text{-}22}$, whereas no contacts with $N54^{IL\text{-}22}$ are observed in the other solutions. Finally, $Y173^{sIL\text{-}10R2}$ forms an extensive hydrogen bond network in C-B-R-15-S6, which is consistent with the reduced binding properties of $Y173A^{sIL\text{-}10R2}$ for IL-22/sIL-22R1.

In contrast to experiments performed with IL-22/sIL-22R1, sIL-10R2 docking to cmvIL-10/sIL-10R1 identified a single solution, found only using chain B, which fit the evaluation criteria (C-B-R12-S1, Fig S6, Table S2). Not only was the cmvIL-10/sIL-10R1/sIL-10R2 C-B-R12-S1 structure consistent with the sIL-10R2 mutagenesis data, but it also shares similar contacts when compared to the IL-22 ternary complex docking solution, C-B-R15-S6. In particular, $Y59^{sIL\text{-}10R2}$ forms similar contacts with helix D in both complexes and $R60^{sIL\text{-}10R2}$ is positioned to form salt bridges with conserved glumate residues ($E101^{IL\text{-}22}$ and $E74^{cmvIL\text{-}10}$) in each complex. For IL-22/sIL-22R1 and cmvIL-10/sIL-10R1, the best solutions were both obtained from docking experiments performed with sIL-10R2 chain B. The D1/D2 inter-domain angles differ as described in Figure S2 between the non-crystallographic chains (chain A and B). In Figure S2, we also compare the domain angles of the IL-10R2 chains A and B against the final IL-10R2 models docked onto the IL-22/sIL-22R1 and cmvIL-10/sIL-10R1 complexes (Table S2). This comparison shows the inter-domain angle of sIL-10R2s in the final docking models are almost identical to the sIL-10R2 chain B crystal structure (Fig S2C). In contrast, docking models generated with chain A (Table S2) show considerable deviations away from the starting sIL-10R2 chain A crystal structure (Fig S2B). In practical terms, this corresponds to a ~10° movement of D2 towards (sIL-10R2 chain A) or away (sIL-10R2 chain B) from the D2 domains of sIL-10R1 and sIL-22R1 in the ternary complexes (Figs 4 and 5). Overall, the data suggests chain B reflects the preferred sIL-10R2 D1/D2 orientation required to assemble IL-22 and IL-10 ternary complexes. However, it is possible that the optimal D1/D2 orientation is somewhere within the range of sIL-10R2 domain angles observed in the crystal.

Supplemental References:

Jones, B.C., Logsdon, N.J., and Walter, M.R. (2008). Structure of IL-22 bound to its high-affinity IL-22R1 chain. Structure *16*, 1333-1344.

Deivanayagam, C.C., Rich, R.L., Carson, M., Owens, R.T., Danthuluri, S., Bice, T., Hook, M., and Narayana, S.V. (2000). Novel fold and assembly of the repetitive B region of the Staphylococcus aureus collagen-binding surface protein. Structure Fold Des *8*, 67-78.

Logsdon, N.J., Jones, B.C., Allman, J.C., Izotova, L., Schwartz, B., Pestka, S., and Walter, M.R. (2004). The IL-10R2 binding hot spot on IL-22 is located on the N-terminal helix and is dependent on N-linked glycosylation. J Mol Biol *342*, 503-514.

McDonald, I.K., and Thornton, J.M. (1994). Satisfying hydrogen bonding potential in proteins. J Mol Biol *238*, 777-793.

Wolk, K., Witte, E., Reineke, U., Witte, K., Friedrich, M., Sterry, W., Asadullah, K., Volk, H.D., and Sabat, R. (2004). Is there an interaction between interleukin-10 and interleukin-22? Genes Immun.

Wu, P.W., Li, J., Kodangattil, S.R., Luxenberg, D.P., Bennett, F., Martino, M., Collins, M., Dunussi-Joannopoulos, K., Gill, D.S., Wolfman, N.M., and Fouser, L.A. (2008). IL-22R, IL-10R2, and IL-22BP binding sites are topologically juxtaposed on adjacent and overlapping surfaces of IL-22. J Mol Biol *382*, 1168-1183.

Yoon, S.I., Logsdon, N.J., Sheikh, F., Donnelly, R.P., and Walter, M.R. (2006). Conformational changes mediate interleukin-10 receptor 2 (IL-10R2) binding to IL-10 and assembly of the signaling complex. J Biol Chem *281*, 35088-35096.